
Jet, Wave, and Droplet Velocities for a Continuous Fluid Jet

Randy Fagerquist

Scitex Digital Printing, Inc., Dayton, Ohio

Abstract

This paper presents data showing the relationship of the jet velocity (V_j), λf , and the droplet velocity (V_d) of a continuous, stimulated jet emanating from an orifice in a thin, flat plate. The jet velocity measurement is non-trivially derived from the flow rate, as the jet diameter (D) is a function of V_j due to the presence of a dynamical meniscus at the orifice-jet boundary. λ is the measured wavelength of the surface deformation imposed on the jet at a frequency, f . The droplet velocity is measured in a straightforward fashion.

We find good agreement between the measured values for λf and those calculated from the simple veloc-

ity potential theory for cylindrical jets for $\lambda/D <_{II}$. However, the same theory predicts $\lambda f = V_j$ and $V_j > V_d$ for $\lambda/D >_{II}$, which we do not find to be strictly true. A possible contributing factor for this discrepancy includes the fact that the surface deformation along the length of the stimulated jet, in this case, is a monotonically increasing amplitude, culminating in droplet formation and break-off. This strongly violates the assumption of a uniform and infinitesimal deformation in the simple theory.

Introduction

The physics of liquid jet surface deformations is of great interest in the continuous ink jet field due to the fundamental role it plays in determining droplet generation for the printing process. As the sophistication and requirements for speed increase, there is a constant need for higher frequency droplet generation and break-off uniformity. This work is aimed at furthering our under-

standing of the fluid physics and dynamics of the stimulated fluid jet and droplet generation.

One of the questions which has become more important recently is how the large amplitude deformations behave as compared to the more well-known and understood small amplitude deformations. Rayleigh¹, of course, addressed the basic problem of the infinite liquid cylinder with an imposed uniform surface perturbation. He was able to show many of the salient features of the jet deformation growth as a function of time. In reality, however, the liquid jets used for ink jet printing do not have infinite extent and do not have small perturbations imposed on the surface. The jets, in a properly operating printer, have relatively short length before breaking up into droplets. This is accomplished by imposing a substantial surface deformation on the jet as it exits the orifice.

Our experimental work was carried out using printhead components from the Scitex 5100 printer. The droplet generators had 132 jets that emanated from orifices having diameters ranging from 1.86-to-1.88 mils. The printhead test stand was equipped to provide wide range frequency stimulation of the jets and variable fluid pressure. A proprietary liquid ink with well-known fluid properties was used as the test fluid.

An LED strobe light source, a microscope and reticule; and a Mideo Systems video imaging system with Media Cybernetics ImagePro Plus analysis software were used to record the jet surface deformations during the course of the experiment. Data analysis, preparation, and presentation was accomplished with ImagePro, MS-Excel, and MS-Word software.

Jet Velocity

In principle, the velocity of an unstimulated jet is easily determined from the flowrate, Q , and jet diameter, D by:

$$V_j = \frac{4Q}{\rho\pi D^2}. \quad (1)$$

The average flowrate, Q , of a jet at each test pressure was measured by collecting the jetted fluid of 132 individual jets for a known amount of time and weighing it. The fluid pressure was electromechanically controlled to better than ± 0.05 psi. This procedure was performed several times for each condition so that an average value of the flowrate was obtained—not only for many jets at once, but also over a time of several tens of seconds.

The density of the fluid used for these experiments was determined at the time of manufacture and was checked periodically during the experiments. The fluid supply was also routinely replaced during the course of the experimentation, so that any variations of the data due to fluid density fluctuations could be kept minimal.

A typical result is shown as a plot of Q vs. $P^{1/2}$ in Figure 1. Plotted this way, the flowrate is shown to be linear w.r.t. $P^{1/2}$. Since V_j is related to Q by (1), then $V_j \sim P^{1/2}$ holds true for the case of $D=\text{constant}$ —which is predicted by simple theory. However, D is found to be a function of

V_j ,² and for the lower flowrates (pressures), can be significantly different from the diameters at larger flowrates.

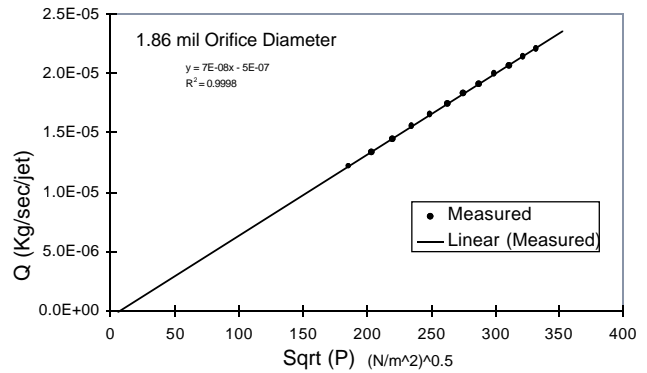


Figure 1. Single Jet Flowrate vs. the Square Root of the Pressure

In practice, if one assumes the value of D is the same as the orifice diameter, and if D , ρ , and Q are measured with an accuracy of, say, 1%, then the error for V_j is on the order of 4%. This error is compounded if the variation of the jet diameter as a function of flowrate is not accounted for, making an independent measurement of D necessary for the range of pressures investigated here.

Measurements of D vs. the fluid pressure, P , were made using two different set-ups. The first method employed a strobe light source backlighting the jet array and a photodetector in conjunction with a microscope focus on a portion of the jet array. The jets were imaged onto the photodetector which was connected to a lock-in amplifier referenced to the strobe source. When the pressure of the fluid behind the orifice plate was varied, the diameters of the jets changed in concert with the jet velocity, causing the “shadow” cast by the jets on the detector to vary proportional to the changing diameters. This caused the output of the detector to increase or decrease accordingly, which was then amplified with a high signal-to-noise ratio by the lock-in. The output voltage of the lock-in was, in this set-up, proportional to the average diameter of the jets in view of the microscope.

This method of measuring the jet diameter had the disadvantage of being difficult to calibrate and sensitive to detector and light source drift. It also was generally used with low power microscope magnification of the jets and, therefore, the results are values of D that are averages over several individual jets. This method has the advantage of having almost infinite resolution, with the detector output being an analogue signal proportional to the amount of light striking it.

The second method of jet diameter measurement was direct analysis of the video images of highly magnified, unstimulated jets made with the Mideo video system. Many individual measurements of several jets for each trial were made and averaged, producing an average diameter for a single jet.

Since the jet images were made with the video system having two jets always in the field-of-view, and since the jet spacing for the arrays used were very well known, these images were self-calibrating. This proved to be a big advantage over the lock-in method, where absolute calibration was

difficult to achieve. The major disadvantage the video method had was that, because the captured images were digital, the resolution of the D measurements were inferior to that provided by the lock-in method. This was partially compensated for by making many such images and measurements and finding an average value for a jet diameter.

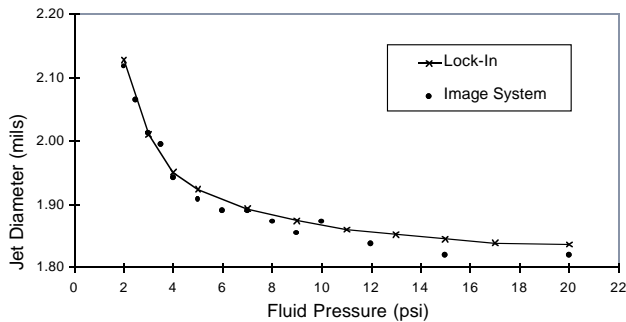


Figure 2. Average Single Jet Diameter vs. Pressure

The relationship between D and V_j is shown by Figure 2, where data provided by both methods of measurement are shown. As can be seen, at low pressures and jet velocities, the diameter of the jet is found to increase rapidly as P decreases towards 0 psi. As the pressure increases, the jet diameter changes very slowly and appears to approach an asymptotic lower limit. Note that the calibration of the lock-in curve was determined by the video measurements of D .

With Q , D , and ρ being known (measured) quantities, the values for V_j were calculated from (1). Many of these results are found in Table 1 and are addressed in the Results and Discussion section.

Droplet Velocity

The droplets that form from the break-up of the jets travel with a velocity parallel to the jet velocity. The magnitude of the droplet velocity was measured by using a stroboscopic light source backlighting the array of droplets after break-off so that they appear fixed in space. A microscope with reticule or a video image and of the array can be used to determine the spacing of the droplets in the direction of travel. Knowing the frequency of jet stimulation, f_s , allows the droplet velocity, V_d , to be calculated from

$$V_d = f_s \cdot L \quad (2)$$

where L is the droplet spacing in the direction of the velocity.

A typical video image of an array of droplets in flight used for measuring L , is shown in Figure 3. The droplets are moving downward in the figure, as indicated in the figure, and are shown over a distance of about $6L$. An artifact of the droplet break-off process is visible in the figure as a periodic distortion of the droplets from perfect spherical shapes. The row of droplets near the center of the figure are somewhat flattened as compared to the row just above or below it. The first and last two rows show droplets which are elongated in the vertical

direction. This is typical of the oscillating droplet geometry that is often observed immediately below the break-off point.

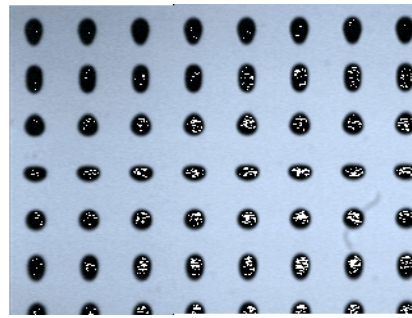


Figure 3. Droplets in Flight After Break-off

Even though the droplet shape is oscillating, the velocity of the center of mass is constant. Therefore, when making measurements of the droplet position—either with the microscope reticule or video image analysis software—it is the center of droplet mass that was located. One way to minimize the error encountered locating the center of mass visually is to measure the distance between two widely separated droplets in the vertical direction and dividing the distance by the number of spacings.

Video images, like the one shown as Figure 3, were analyzed with an image analysis computer program. This program had several advanced features, including one that determined the position of the droplet centroids in the x and y directions. The differences between neighbor droplet centroids in the velocity direction is L , from which V_d can be determined from (2), above.

Some care was given to make the droplet velocity measurements near the point of break-off so that aerodynamic drag did not slow the droplets enough to cause an error in the measurement of L . On the other hand, if the measurements are attempted too close to the break-off point, the position of the droplet center of mass becomes more difficult to determine due to the large distortion of the droplet shape there. Generally, our droplet velocity measurements were made on an array of droplets a few L below the break-off point to minimize the effects of air drag and distorted droplet geometry.

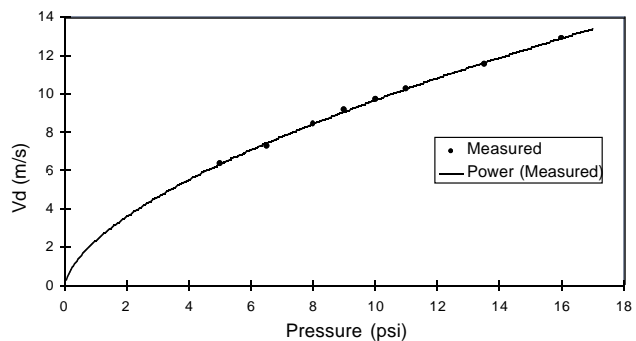


Figure 4. Droplet Velocity vs. Pressure

The result of a typical series of measurements is shown as Figure 4, where V_d is plotted as a function of Pressure, P . The solid line is a power law fit of the form $V_d = aP^x$, where a and x are fitted parameters. Additional measurements of droplet velocity are listed in Table 1 and are discussed further in the Results and Discussion section.

Wave Velocity

Small Amplitude Waves

The most interesting of the three velocities studied here is the wave velocity. Rayleigh¹, of course, in his early pioneering work, studied the problem of small amplitude perturbations on an infinite cylindrical jet. He found that there were two regimes for the surface of the jet which are separated by the value of λ/D , where λ is the wavelength of the disturbance and D is the diameter of the jet.

The simplest form of the problem is considered here, where:

- (1) the fluid is considered inviscid
- (2) the flow is irrotational: $\vec{\nabla} \times \vec{V} = \vec{\nabla} \cdot \vec{V} = 0$
- (3) the fluid density $\rho = \text{constant}$
- (4) the $\frac{1}{2}\rho V^2$ term in Bernoulli's equation is negligible compare to the others
- (5) and the velocity potential, ϕ , is defined by:

$$-\frac{\partial \phi}{\partial r} = V_r, \quad -\frac{\partial \phi}{\partial z} = V_z, \quad \vec{\nabla} \phi = \vec{V}$$

The differential equation for this problem is the cylindrical Laplacian:

$$\frac{\partial^2 \phi}{\partial r^2} + \frac{1}{r} \frac{\partial \phi}{\partial r} + \frac{\partial^2 \phi}{\partial z^2} = 0. \quad (3)$$

Assuming a product solution of the form:

$$\phi = R(r)Z(z)T(t),$$

and the boundary conditions:

$$V_r(R) = \frac{dR}{dt} = -\frac{\partial \phi}{\partial r} \text{ at } r = R; \text{ and } \frac{\partial R}{\partial z} \ll 1;$$

so that the curvature at the surface of the jet is, to a good approximation, given by:

$$\frac{\partial^2 R}{\partial z^2} \approx \frac{\frac{\partial^2 R}{\partial z^2}}{\left[1 + \left(\frac{\partial R}{\partial z}\right)^2\right]^{3/2}}.$$

These approximations, conditions, and restrictions then allow a simple harmonic solution to (3), with the dispersion relation:

$$\omega^2 = \left[(k^2 r_0^2 - 1) \left(\frac{k}{r_0^2} \right) \frac{I_1}{I_0} \right] \frac{\sigma}{r}, \quad (4)$$

where σ = surface tension of the fluid, ρ = fluid density, r_0 = unperturbed jet radius, $k = 2\pi/\lambda$, $\omega = 2\pi f$, and I_1 and I_0 are the usual Bessel functions.

When $kr_0 > 1$ ($\lambda/D < \pi$), ω is real and positive and represents the angular frequency of a wave on the surface of the jet propagating with a phase velocity, $V_p = \omega/k$. (Note that the relation (4) also yields the proper results for the propagation of plane waves on the surface of a level liquid by taking the limits $k, r_0 \rightarrow \infty$.)

When $kr_0 < 1$, then ω becomes imaginary and describes the case where the amplitude of the disturbance grows as a function of time at an exponential rate—but at rest w.r.t the fluid. That is, the disturbance only grows in amplitude and does not propagate along the length of the jet.

An example of the wave propagation mode, $kr_0 > 1$, on the surface of a liquid jet is shown as Figure 5. The amplitude of the disturbance does not increase in the jet velocity direction and has a wavelength such that $\lambda/D < \pi$. It eventually damps out due to fluid viscosity, which was not included in the analysis here.



Figure 5. Stimulated Jets with $\omega/D < \pi$.

Figure 6 shows a jet stimulated such that $\lambda/D > \pi$, or $kr_0 < 1$. The amplitude of the disturbance clearly increases in the direction of the jet velocity, until about 6λ from the origin, the amplitude reaches the magnitude of the jet radius itself. When this point is reached, the jet breaks up and droplets form.

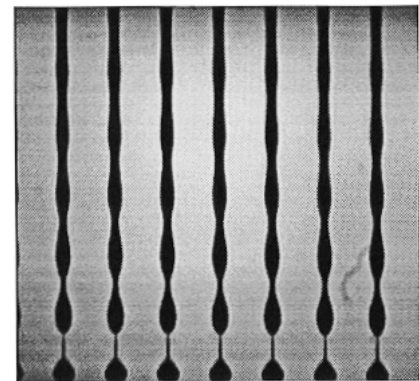


Figure 6. Stimulated Jets with $\lambda/D > \pi$

Many measurements of $V_w = \omega/k$ and V_d were made at a number of λ/D values. The difference between ω/k and V_d were calculated and are plotted in Figure 7.

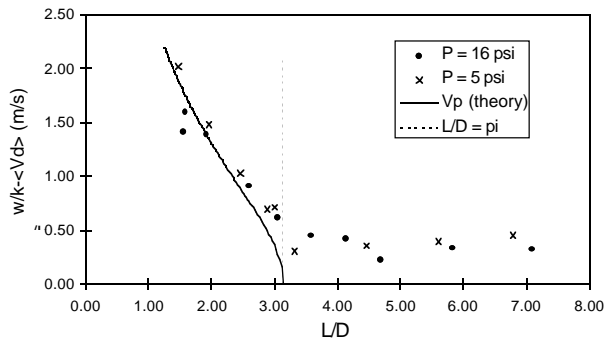


Figure 7. $\omega/k - \langle V_d \rangle$ vs. λ/D

The line to the left of $\lambda/D = \pi$ is calculated from the dispersion relation (4) with the proper parameters for the test conditions used. As can be seen from the plot, the theoretical calculation for the phase velocity is very close to the measured values. To the right of $\lambda/D = \pi$, the value of $\omega/k - V_d$ is roughly constant and slightly larger than zero.

Large Amplitude Waves

When the amplitude of the disturbance on the jet is no longer small enough to satisfy the boundary conditions and approximations discussed above, then the solutions to (3) are likely to be less able to properly describe the wave motion or disturbance growth that takes place. A large amplitude disturbance can be obtained by allowing a true perturbation to grow until the surface variation becomes on the order of the jet radius, as in Figure 6 above; or have a large amplitude initial disturbance, as shown in Figure 7.



Figure 8. Large Amplitude Initial Disturbance

The large amplitude initial disturbance condition in Figure 8 shows that, under these conditions, the jets break up into droplets at a distance of about 3λ from the origin. A jet surface line profile of a similar large disturbance is shown as Figure 9.

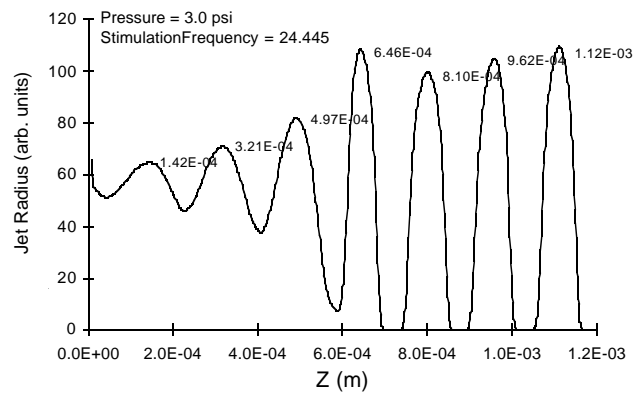


Figure 9. Surface Profile of Large Initial Disturbance Jet

The numbers near the curve in the figure are the values for z of the radial maxima, where the axis of the jet lies along the Z -axis. The jet breaks up into droplets at $Z \approx 7 \times 10^{-4}$ m and the profile of the droplets is plotted to the right of this point.

In Figure 10, the Z -values of the maxima are plotted vs. position for both the wave and droplets. The slopes of the fitted lines for each are the velocities for each: $V_d = 3.85 \pm 0.04$ m/s and $V_w = 4.32 \pm 0.04$ m/s. The difference between the droplet and wave velocities is thought to be due to a retarding force acting on the break-off droplet during the last period for which the droplet is still connected to the jet³.

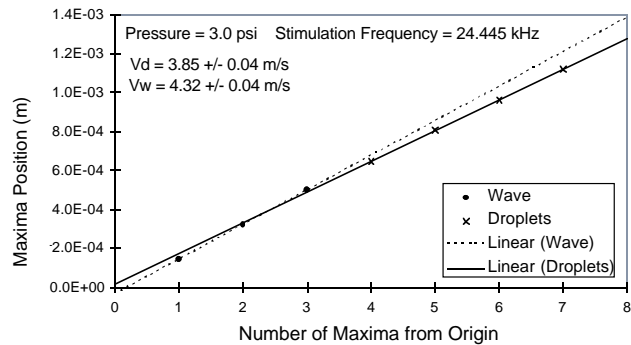


Figure 10. Wave Maxima vs. Distance from Origin: 3.0 psi

Figure 11 shows a similar plot for the maxima from a 9.5 psi (faster) stimulated jet. The wave velocity of the maxima, $V_w = 9.17 \pm 0.23$ m/s, is close to the velocity for the droplets of 9.00 ± 0.04 m/s. However, as tabulated in Table 1, the average V_w for 9.5 psi jets is $\langle V_w \rangle = 9.53 \pm 0.06$ m/s. The large error for the V_w calculated from the points in the figure is, in fact, not an actual error, but rather is due to the maxima not being linearly spaced along the length of the jet. The value for $\langle V_w \rangle$ in Table 1 was obtained from the average of a large number of measurements for *small amplitude* disturbance stimulation for 9.5 psi jets at 3 different stimulation frequencies.

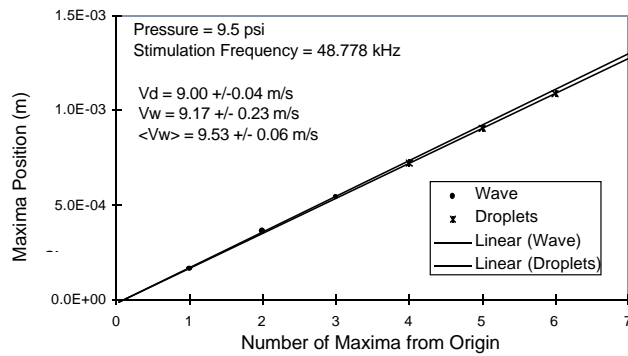


Figure 11. Wave Maxima vs. Distance from Origin: 9.5 psi

Results and Discussion

The results from the previous section point out one of the anomalies encountered with large amplitude stimulation: the wave velocity appears to depend on the jet velocity in some cases, and/or is possibly not well-defined in others. Amplitude-dependent wave velocity and propagation are characteristic of the non-linear effects in fluid dynamics.

A closer examination of the high amplitude surface deformation reveals that the wavelength of the wave is not truly constant. Figure 12 is a plot of the wave maxima positions along Z for the wave on the jet and the first two free droplets.

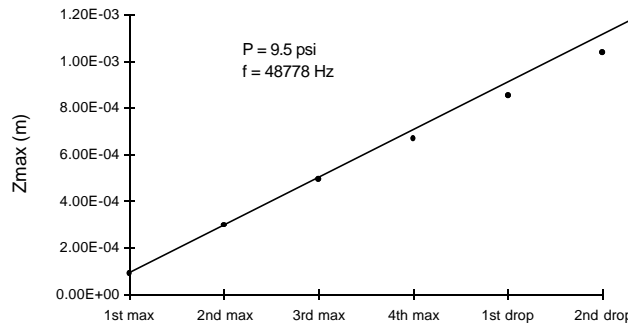


Figure 12. Position of Maxima Along Jet

The dotted line is drawn in the figure to connect the first two points on the left and shows that the subsequent points fall successively farther from the line. Taking the differences between adjacent Z and dividing by the period of stimulation yields the velocity of the wave maxima/droplet averaged over one λ . A plot of these velocities for a 9.5 psi jet stimulated at 48.778 kHz is shown in Figure 13.

The variable wavelength nature of the wave on the jet is apparent in this plot, showing that the local velocity dips sharply near the break-off point, and then increases again to the (constant) droplet velocity. Similar behavior is exhibited by the 3.0 psi, 24.445 kHz data plotted in Figure 14.

These data appear to indicate that the disturbance on the surface of the jet is slowing down as it approaches the break-off point. Once the newly forming droplet has broken off from the main jet, it assumes a constant velocity.

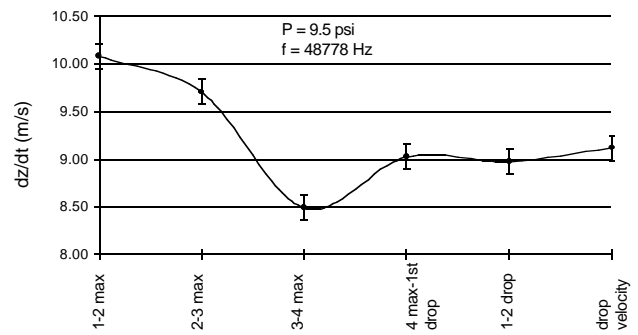


Figure 13. Wave Velocity Profile on Highly Stimulated Jet: 9.5 psi

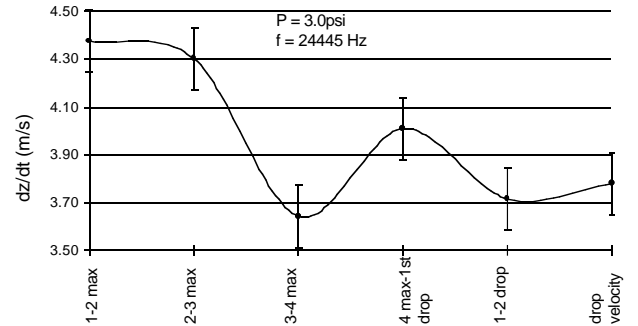


Figure 14. Wave Velocity Profile on Highly Stimulated Jet: 3.0 psi

One implication of this result (that V_w is not constant along the length of the stimulated jet) is that V_w is probably not equal to V_j . It is difficult to say this with certainty, as local measurements of V_j have not been performed. It is likely that local velocities in the continuous region of the stimulated jet are not well-represented by the average velocities, which have been measured here. It can be said that V_w on the continuous portion of the large amplitude stimulated jet and the average value of V_j are not equal.

The overall behavior of the wave and the break-off process found here seems to be consistent with prior analyses in that there is an *apparent* reduction in the fluid momentum in the droplet break-off region. What has actually been determined experimentally is that the *wave* on the jet is retarded near break-off, which is also the point where the amplitude of the stimulation becomes of the same order as the jet radius. The relationship between V_w and V_j is not revealed by this analysis.

Large Amplitude Wave Growth

The rate at which the perturbation on the surface of the jet grows was determined by Rayleigh to be an exponential function of time for $\lambda/D > \Pi$. As discussed before, once the amplitude of the wave on the jet becomes too large for the conditions leading to the dispersion relation (4), then the simple theory probably does not describe the physics well.

In Figure 15, the radius of the jet is measured as a function of time for one period at a fixed position along Z. $R(t)$ in this plot is a periodic function, but not described by a single frequency component⁵.

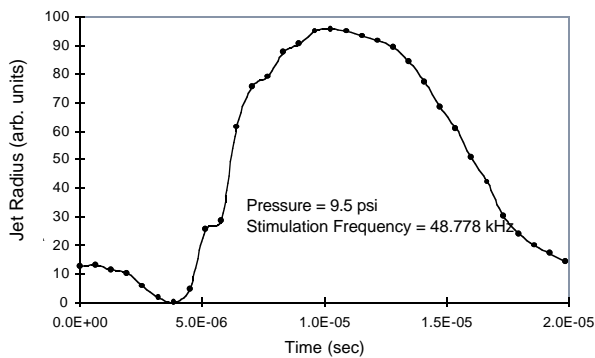


Figure 15. Stimulated Jet Radius vs. Time

It is of interest to calculate the square of the time averaged radius, $\langle R \rangle^2$, and of the square of the radius, $\langle R^2 \rangle$; for comparison purposes.

If the jet velocity at a particular point along the axis of the jet is assumed to be constant w.r.t time, then $\langle Q \rangle = DBV_j \langle R^2 \rangle$. The value of $\langle R^2 \rangle$ vs. Z is plotted in Figure 16, along with the value of $\langle R \rangle^2$.

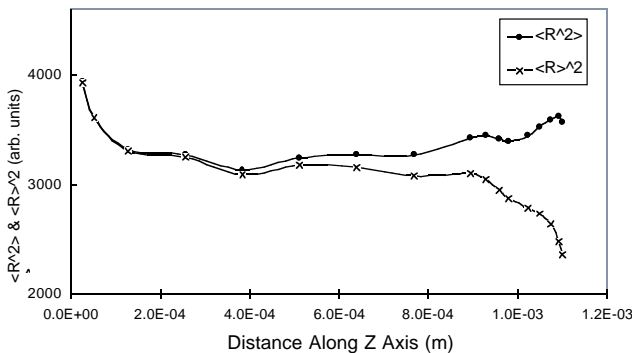


Figure 16. $\langle R^2 \rangle$ & $\langle R \rangle^2$ vs. Z

At first glance, the data plotted in this figure appear to be quite noisy and, not unexpectedly, $\langle R^2 \rangle$ does not equal $\langle R \rangle^2$. However, when the difference $\langle R^2 \rangle - \langle R \rangle^2$ is taken and plotted vs. the same Z values, the resulting curve is quite smooth and is closely described by a simple exponential function, as can be seen in Figure 17, below.

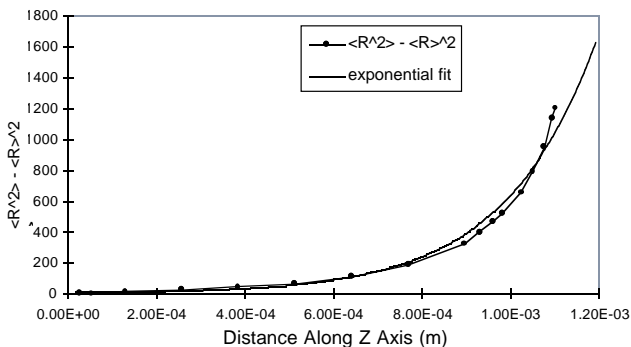


Figure 17. $\langle R^2 \rangle - \langle R \rangle^2$ vs. Z

The resulting smoothness of the curve in this plot is surprising considering the fluctuations in the data of Figure 16. This shows that the details in the plot of $\langle R^2 \rangle$

and $\langle R \rangle^2$ are real and not noise. The difference data also show that the amplitude disturbance grows with time in an exponential fashion.

If the time dependent radius can be written as $R(t) = R_0 + r(t)$, where $r(t)$ is a periodic function of time and $\langle r \rangle = 0$, then $\langle R^2 \rangle - \langle R \rangle^2 = \langle r^2 \rangle$. It follows that $\langle r^2 \rangle$ grows exponentially with time. If $r(t) = r_0 \cos(Tt)$, then $\langle r^2 \rangle = r_0^2/2$, so that the amplitude, r_0 , is found to grow exponentially.

Measurements of V_j , V_w , & V_d

An extensive series of measurements were made using the video imaging system of the wavelength of the jet disturbances and droplet positions in order to obtain relatively accurate values for V_w and V_d . These measurements were made for 3.0 and 9.5 psi fluid pressures. The 9.5 psi trials were repeated for stimulation frequencies of 32.663, 48.778, and 67.113 kHz. The 3.0 psi trial used a stimulation frequency of 24.442 kHz.

The average jet flowrate was measured together with a video system measurement of the unstimulated jet radii. These measurements, along with the known value for the fluid density, then allow calculation of the average jet velocity, V_j . The results of these measurement are recorded in Table 1. Note that there is only a single value of V_j for each pressure. All of the individual V_j measurements were averaged together since no dependence on stimulation frequency is possible for this velocity.

Figure 18 is a plot of the 9.5 psi data from Table 1, where the velocities are plotted vs. their values of λ/D . This figure reveals that the wave velocity is significantly larger than the droplet velocity and that both dip slightly as λ/D approaches Π . The large error bars for the jet velocity prohibit any strong statements concerning the magnitude of V_j . It appears from these data that the jet velocity is comparable to the droplet velocity and is substantially less than the wave velocity. Only more precise measurements of V_j will bear this out.

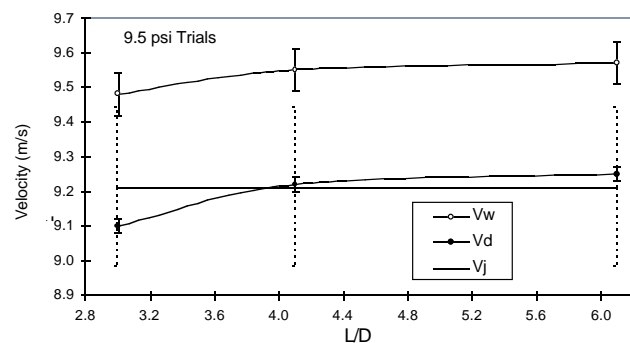


Figure 18. V_w , V_d , & V_j vs. λ/D for 9.5 psi

Conclusions

The problem of waves on a cylindrical jet has a straightforward solution only when the amplitude of the deformation is small. Small deformation waves were generated for $\lambda/D < \Pi$. The phase velocity of these waves as a function of λ/D were found to be in good agreement

Table 1.

Pressure	Stim. Freq	Q	D	8/D	V _w	V _d	V _j
(psi)	(kHz)	(10 ⁻⁶ kg/sec)	(10 ⁻⁵ m)		(m/s)	(m/s)	(m/s)
3.0	24.442	9.130" 0.003	5.28" 0.05	3.3	4.20" 0.07	3.78" 0.03	4.12" 0.05
9.5	32.663	16.90" 0.03	4.79" 0.10	6.1	9.48" 0.04	9.10" 0.02	9.21" 0.23
9.5	48.778	"	"	4.1	9.55" 0.08	9.22" 0.02	"
9.5	67.133	"	"	3.0	9.57" 0.06	9.25" 0.02	"

with the dispersion relation, (4) (see Figure 7). This dispersion relation came from the solution of (3) with many simplifying assumptions and approximations. When these simplifications are not allowed, as is the case when the amplitude of the wave motion becomes large, the solutions become less useful in describing the actual wave motion on the jet.

The deviation from simple theory of the wave when the surface deformation is large was revealed in the measurements of the wave propagation along the length of the jet for $\lambda/D > \Pi$. We found that the wavelength of the large amplitude deformation decreased as the amplitude increased in the direction of the jet velocity. This suggests that: 1) the jet and wave velocities are probably not the same, as is often assumed, and 2) the wave velocity decreases as the amplitude of the wave increases, until droplet break-off occurs.

The droplet velocity was shown, without question, to be less than the wave velocity on the jet before break-off. Schneider³ and Lienhard⁴ considered the problem and found that the droplet velocity should be less than the jet velocity due to surface tension effects during the period just before break-off. In both cases, however, it was assumed in the analyses that the jet velocity and wave velocity were the same when $\lambda/D > \Pi$. It appears from the measurements made here, that this may not be strictly true. It would not be surprising to find the non-linear nature of the fluid dynamics of this problem to become important when the amplitudes of the surface deformations are no longer small.

Measurements of the jet radius, R, as a function of time at constant Z showed that the radial motion of the surface of the jet is not simple periodic⁴. The time averaged values of R² and R were used to show that the

growth of the deformation amplitude is still roughly an exponential function of time, when the amplitude is defined as $r_0 = [\langle R^2 \rangle - \langle R \rangle^2]^{1/2}$, even though there is a more complicated dependence of the individual values of $\langle R^2 \rangle$ and $\langle R \rangle^2$ on Z.

Another problem of a more experimental nature that proved to be non-trivial, is that of the dependence of the jet radius on jet velocity. This makes the measurement of jet velocity somewhat more complicated and requires an extremely accurate measurement of the jet radius for each trial where the jet velocity is varied in order to maintain a reasonable error for V_j. Even with the high resolution video system measurements, where the radius measurement errors were quite small, the jet velocity measurement could still not be made routinely with less than an error of a few percent—which is large compared to the errors associated with the droplet and wave velocity measurements. More accurate measurements of the jet velocity would have to be made before comparison of the wave and jet velocities can be made with more confidence.

References

1. Lord Rayleigh, *Proc. Roy. Soc.*, **29 71** (1979).
2. R. Fagerquist, *Proc. IS&T's 7th Int'l Congress on Adv. in Non-Impact Printing Technologies*, October 1991, pp. 67-75.
3. J. Schneider, Internal Memo, Scitex Digital Printing, Inc., July 1992.
4. J. H. Lienhard V, J.H. Lienhard (IV), *J. of Fluids Eng.*, **106**, pp.13-17, (1984).
5. A. Soucemarianadin, J. Xing, P. Attane, A. Dunand, *Proc. IS&T's 7th Int'l Congress on Adv. in Non-Impact Printing Technologies*, October 1991, pp. 367-375.